

The Inert Doublet Model: an Archetype for Dark Matter

Laura Lopez Honorez, Emmanuel Nezri, Josep F. Oliver, Michel H.G. Tytgat

*Service de Physique Théorique, Université Libre de Bruxelles,
CP225, Bld du Triomphe, 1050 Brussels, Belgium*

Abstract

The Inert Doublet Model (IDM), a two Higgs extension of the Standard Model with an unbroken Z_2 symmetry, is a simple and yet rich model of dark matter. We present a systematic analysis of the dark matter abundance and investigate the potentialities for direct and gamma indirect detection. We show that the model should be within the range of future experiments, like GLAST and ZEPLIN. The lightest stable scalar in the IDM is a perfect example, or archetype of a weakly interacting massive particle.

1 Introduction

Contemporary cosmological observations concur to indicate that the majority of matter in the universe not only does not shine but is not even made of ordinary atoms [1, 2]. Deciphering the nature of this so-called Dark Matter has become one of the most important issue at the frontier of particle physics, astrophysics and cosmology. A profusion of dark particles have been proposed over the years and it is much hoped that present and forthcoming experiments will throw some light on the matter. For a review, see for instance [3, 4].

In the present article we investigate further a rather mundane, although in our opinion quite interesting, form of dark matter. The particle candidate is a weakly interacting massive scalar and it has been advocated recently in [5] and [6, 7]. The framework is that of a two Higgs doublets, H_1 and H_2 , version of the Standard Model with a Z_2 symmetry such that

$$H_1 \rightarrow H_1 \text{ and } H_2 \rightarrow -H_2.$$

All the fields of the Standard Model are even under Z_2 . This model has been first discussed by Deshpande and Ma in [8]. Following [6], we will assume that Z_2 is not spontaneously broken, *i.e.* H_2 does not develop an expectation value. Among other things, the discrete symmetry prevents the appearance of flavour changing neutral currents. The model is definitely not the $\langle H_2 \rangle \rightarrow 0$ limit of a generic two Higgs model like, for instance, the Higgs sector of the MSSM.

The most general, albeit renormalizable, potential of the model can be written as

$$V = \mu_1^2 |H_1|^2 + \mu_2^2 |H_2|^2 + \lambda_1 |H_1|^4 + \lambda_2 |H_2|^4 + \lambda_3 |H_1|^2 |H_2|^2 + \lambda_4 |H_1^\dagger H_2|^2 + \frac{\lambda_5}{2} [(H_1^\dagger H_2)^2 + h.c.]. \quad (1)$$

There is an Peccei-Quinn $U(1)$ global symmetry if $\lambda_5 = 0$. This limit is however not favored by dark matter direct detection experiments (section 2.3).

The $SU(2) \times U(1)$ symmetry is broken by the vacuum expectation value of H_1 ,

$$\langle H_1 \rangle = \frac{v}{\sqrt{2}}$$

with $v = -\mu_1^2/\lambda_1 = 248$ GeV while, assuming $\mu_2^2 > 0$,

$$\langle H_2 \rangle = 0.$$

The mass of the Brout-Englert-Higgs particle (h or Higgs for short) is

$$M_h^2 = -2\mu_1^2 \equiv 2\lambda_1 v^2 \quad (2)$$

while the mass of the charged, H^+ , and two neutral, H_0 and A_0 , components of the field H_2 are given by

$$\begin{aligned} M_{H^+}^2 &= \mu_2^2 + \lambda_3 v^2/2 \\ M_{H_0}^2 &= \mu_2^2 + (\lambda_3 + \lambda_4 + \lambda_5)v^2/2 \\ M_{A_0}^2 &= \mu_2^2 + (\lambda_3 + \lambda_4 - \lambda_5)v^2/2. \end{aligned} \quad (3)$$

For appropriate quartic couplings, H_0 or A_0 is the lightest component of the H_2 doublet. In the absence of any other lighter Z_2 -odd field, either one is a candidate for dark matter. For definiteness we choose H_0 . All our conclusions are unchanged if the dark matter candidate is A_0 instead. Following [6] we parameterize the contribution from symmetry breaking to the mass of H_0 by $\lambda_L = (\lambda_3 + \lambda_4 + \lambda_5)/2$, which is also the coupling constant between the Higgs field h and our dark matter candidate H_0 . Of the seven parameters of the potential (1), one is known, v , and four can be related to the mass of the scalar particles. In the sequel, we take μ_2 and λ_2 as the last two independent parameters. The later actually plays little role for the question of dark matter.

The abundance of H_0 as the dark matter of the universe as well as the constraints from direct detection experiments have been touched upon in the recent literature [6, 7] (see also [9]). In the present article we investigate the potentialities for indirect detection of H_0 using gamma ray telescopes and detectors. For the sake of completeness, we also present a systematic (albeit tree-level) analysis of the abundance of the H_0 in the light of WMAP data, as well as the prospect for direct detection by underground detectors.

Before doing so, we would like to briefly emphasize some of the virtues of this, so-called, Inert Doublet Model (IDM), both in general and for the issue of dark matter in particular. True, the model is *ad hoc*. Also, it does not address any deep issue, say the hierarchy problem. Yet it is a very simple extension of the Standard Model and its phenomenology is nevertheless very rich [5, 6, 10, 11]. In reference [6], Barbieri *et al* considered this model as a way of pushing the mass of the Higgs particle toward the TeV scale, without contradicting LEP precision measurements (see also [10], and section 3.1 of the present paper). Also, in the simplest version discussed here there are no Yukawa couplings to the H_2 doublet, but it is somewhat natural to imagine coupling it to (odd) right-handed neutrinos. This opens the possibility of generating the mass of the SM neutrinos through loop corrections, a mechanism introduced by Ma in [5] and further addressed in a series of papers [12, 13, 14].

As a dark matter candidate, H_0 is not without interest either. It belongs to the family of Weakly Interacting Massive Particles (WIMP) and has been proposed as a dark matter candidate by Ma. The most acclaimed member of this family is certainly the neutralino, the lightest supersymmetric particle (LSP). The supersymmetric extensions of the SM are without doubt very interesting and well motivated but they involve many new parameters and their phenomenology is, to say the least, complex. It is perhaps far fetched to compare the respective advantages and disadvantages of the IDM and of the MSSM but it is interesting that the H_0 shares many similarities with the LSP (weak interactions, similar mass scale, etc) while being considerably much simpler to analyze. Interestingly, if we take seriously the idea that H_0 is the dominant form of dark matter, the parameter space of the IDM model is quite constrained. It is also, to some extent, complementary to that of the MSSM, as we show in the conclusions. And, cherry on the top, the phenomenology of the H_0 as a candidate for dark matter is neatly intertwined with that of the Higgs particle. In our opinion, it is this conjunction of simplicity and richness that makes the lightest stable scalar a perfect example, or archetype, of dark matter.

The plan of the paper is as follow. In the next section (2) we give a summary of our methodology for the calculations of the dark matter abundance, the photon flux for indirect detection by gamma ray telescopes and the cross-sections for direct detection. We then discuss in some details the results of our analysis, in the light of WMAP data, and study the prospects for both indirect and direct detection by existing and forthcoming experiments. We give our conclusions in the last section, together with comparison of the Model with that of the MSSM, and the prospects for future analysis.

2 Dark matter aspects

2.1 Dark Matter abundance

The abundance of H_0 has been estimated in [6] and in [7] for two different mass ranges. As in these papers, we consider only the standard freeze-out mechanism. There are then essentially two regimes, depending on the mass of H_0 with respect to that of the W and Z bosons. If $M_{H_0} \gtrsim 80\text{GeV}$, the H_0 annihilate essentially into Z and W boson pairs (see Figure (1)). For $M_{H_0} > M_h$, the annihilation channel into h pairs opens (see Figure (2)). Otherwise, the H_0 annihilate essentially through an intermediate Higgs, provided the Higgs itself is not too heavy. Some amount of coannihilation of H_0 with the next-to-lightest scalar particle A_0 (resp. H^+) through a Z (resp. W^+) boson can be present [15], a feature that substantially complicates the determination of the dark matter abundance (see Figure (3)).

We have computed the relic abundance of H_0 using micrOMEGAs2.0, a new and versatile package for the numerical calculation of Dark Matter abundance from thermal freeze-out [16]. The latest implementation of this code, which was originally developed to study supersymmetric models, allows one to enter any model containing a discrete symmetry that guarantees the stability of the dark matter particle. The code takes advantage of the fact that each odd (*i.e.* non standard) particles of the model will eventually decay into the lightest odd particle, in our case the H_0 . One can then sum the system of Boltzmann equations of all odd species and the relic density of dark matter is calculated by solving the Boltzmann equation for the lightest particle only [17]:

$$\frac{dY}{dT} = \sqrt{\frac{\pi g_*(T)}{45}} M_{Pl} \langle \sigma v \rangle (Y^2(T) - Y_{eq}^2(T)), \quad (4)$$

where $Y \equiv n_{DM}/s$ is the comoving density of dark matter. All the processes of the model enter in the thermally averaged cross-section $\langle \sigma v \rangle$. Integrating Eq.(4) from $T = \infty$ to $T = T_0$ the relic abundance is given by

$$\Omega_{DM} h^2 = 2.72 \times 10^8 \frac{M_{DM}}{\text{GeV}} Y(T_0). \quad (5)$$

MicrOMEGAs2.0 itself is build upon CALCHEP, a code for computing tree-level cross-sections. We have used both MicrOMEGAs2.0 and CALCHEP to compare with our analytical calculations and to perform a number of cross-checks that have strengthened our faith in the numerical results reported in the present paper.*

2.2 Indirect detection

The measurement of secondary particles coming from dark matter annihilation in the halo of the galaxy is a promising way of deciphering the nature of dark matter. This possibility depends however not only on the properties of the dark matter particle, through its annihilation cross-sections, but also on the astrophysical assumptions made concerning the distribution of dark matter in the halo that supposedly surrounds our galaxy. The galactic center (GC) region is potentially a very attractive target for indirect detection of dark matter, in particular through gamma rays. The produced gamma ray flux from the annihilation of dark matter particles can be expressed as

$$\frac{\Phi_\gamma}{d\Omega dE} = \sum_i \frac{dN_\gamma^i}{dE_\gamma} \langle \sigma_i v \rangle \frac{1}{4\pi m_{DM}^2} \int_{\text{l.o.s.}} \rho^2 dl, \quad (6)$$

where m_{DM} is the dark matter particle mass, ρ is the dark matter density profile, $\langle \sigma_i v \rangle$ and dN_γ^i/dE_γ are, respectively, the thermally averaged annihilation cross section times the relative velocity v and the differential gamma spectrum per annihilation coming from the decay of annihilation products of final state i . The integral is taken along the line of sight. The processes involved are shown in the Figure (3), first diagram and Figures (1) and (2).

*The Feynman rules and definition files of the IDM to be used with micrOMEGAs can be obtained upon request to the authors of the present article and will be included in the next available version of the code.

The models will be constrained by the existing EGRET [18] experimental limit on the flux, $\sim 10^{-8}$ photons $\text{cm}^{-2}.\text{s}^{-1}$, and the forthcoming GLAST [19] expected sensitivity, $\sim 10^{-10} - 10^{-11}$ photons $\text{cm}^{-2}.\text{s}^{-1}$ for $\Delta\Omega = 10^{-3}$ and 10^{-5} sr respectively.

Our purpose for the time being is merely to prospect the IDM with regard to gamma ray indirect detection. In this paper, we focus on the particle physics parameter dependence of the model and work within a fixed astrophysical framework, the popular Navarro-Frank-White (NFW) halo profile [20]. With $R_0 = 8.5$ kpc equal to the distance from Sun to the GC and $\rho_0 = 0.3 \text{ GeV}.\text{cm}^{-3}$ the dark matter density in our neighborhood, the NFW profile density can be parameterized as

$$\rho(r) = \rho_0 \frac{[1 + (R_0/a)^\alpha]^{(\beta-\gamma)/\alpha}}{[1 + (r/a)^\alpha]^{(\beta-\gamma)/\alpha}} \left(\frac{R_0}{r}\right)^\gamma, \quad (7)$$

with $(a, \alpha, \beta, \gamma) = (20, 1, 3, 1)$. It should be emphasized that the (dark) matter distribution in the innermost region of the galaxy is poorly known so that γ is not very constrained, a freedom that can give rise to very different values of the gamma ray flux. Typically a suppression or an enhancement of two orders of magnitude can be obtained if one considers respectively a halo with a flat core (*e.g.* isothermal, $\gamma = 0$) or a deeper cusp ($\gamma \sim 1.5$) [21] coming for instance from baryonic infall. Hence, depending on the astrophysics assumptions, the estimation of gamma ray signal can vary quite strongly (see *e.g.* [23, 22]).

To calculate the flux we have integrated (6) for a NFW profile above 1 GeV and around a solid angle of $\Delta\Omega = 10^{-3}$ sr for EGRET and $\Delta\Omega = 10^{-5}$ sr for GLAST. The differential spectra of each channel are given by micrOMEGAs (we have checked the agreement with Pythia simulations of [23]) as well as $\langle\sigma v\rangle$ at rest and we have integrated the square of the dark matter density along the line of sight.

2.3 Direct detection

A local distribution of weakly interacting dark matter could be detected [24] by measuring the energy deposited in a low background detector by the scattering of a dark matter particle with a nuclei of the detector. One distinguishes spin dependent and spin independent interactions. For H_0 interacting with the quarks of the nuclei, there are two spin independent processes at tree level, $H_0 q \xrightarrow{Z} A_0 q$ and $H_0 q \xrightarrow{h} H_0 q$ (see Figure (4)). The experiments have reached such a level of sensitivity that the Z exchange contribution is excluded by the current experimental limits. Consequently, to forbid Z exchange by kinematics, the mass of the A_0 particle must be higher than the mass of H_0 by a few 100 keV (we will thus disregard the $\lambda_5 \rightarrow 0$ limit). We assume that the main process here is the one with Higgs particle exchange h . The cross section at tree-level is [6]

$$\sigma_{H_0-p}^h = \frac{m_r^2}{4\pi} \left(\frac{\lambda_L}{M_{H_0} M_h^2}\right)^2 f^2 m_p^2, \quad (8)$$

where f is a form factor estimated in the literature to be $f \sim 0.3$ and m_r is the reduced mass of the system. [25]. In addition, for $M_{H_0} < M_W$, we have neglected the one-loop exchange of two gauge bosons. For $M_{H_0} > M_W$, we include this process with, following [7], $\sigma_{H_0-p} \simeq 4.6 \cdot 10^{-13} \text{ pb}$. We take into account the constraints given by the CDMS [26] experiment ($\sim 10^{-6} \text{ pb}$) and the model is also compared to the next generation experiments like EDELWEISS II [27] or a ton-size experiment like ZEPLIN [28] with the valley of their sensitivities respectively around $\sigma \sim 10^{-8}$ and $\sigma \sim 10^{-10} \text{ pb}$.

3 Analysis

The processes driving the (co)annihilation cross section $\langle\sigma v\rangle$ relevant for the relic density from freeze-out and indirect detection of gamma rays are shown in the Figures (1), (2) and (3). The H_0 -proton interactions relevant for direct detection are shown in Figure (4).

There are two qualitatively distinct regimes, depending on whether the H_0 is lighter than the W and Z and/or the Higgs boson, in which case annihilation proceeds through the diagrams of Figure

(3). At low mass, the second diagram of (3) may contribute to the dark matter abundance if there is a substantial number of A_0 at the time of freeze-out (*i.e.* coannihilation).

In the plots of Figure (5), the relic abundance of H_0 dark matter particles, the gamma ray flux due to H_0 annihilation at the galactic center (indirect detection) and, finally, their cross-section for elastic scattering off a proton through Higgs boson σ_{H_0-p} (direct detection) exchange are shown, for two particular Higgs masses ($M_h = 120$ GeV and 200 GeV) in the (M_{H_0}, μ_2) plane. We refer to this as the low H_0 mass regime. For higher H_0 masses, similar plots are displayed in Figure (6) (for $M_h = 120$ GeV), respectively for the dark matter abundance, the gamma ray flux and the cross-section for direct detection. In each of these three cases, the color gradients correspond respectively to gradients in $\log(\Omega_{H_0} h^2)$, $\log(\Phi_\gamma (\text{cm}^{-2}\text{s}^{-1}))$ and $\log(\sigma_{H_0-p}(\text{pb}))$.

Since we plot our results in the (M_{H_0}, μ_2) plane, the diagonal line corresponds to $\lambda_L = 0$, *i.e.* to no coupling between H_0 and the Higgs boson. Away from this line, λ_L increases, with $\lambda_L < 0$ (resp. $\lambda_L > 0$) above (resp. below) the diagonal. Also, we write $\Delta M A_0 = M_{A_0} - M_{H_0}$ and $\Delta M H_c = M_{H^+} - M_{H_0}$.

In the plots of the dark matter abundance, the areas between the two dark lines correspond to regions of the parameter space such that $0.094 < \Omega_{DM} h^2 < 0.129$, the range of dark matter energy densities consistent with WMAP data. In the cross section and gamma ray flux plots, the lines indicate the areas of the parameter space within reach of the various experiments we take in consideration.

3.1 Constraints

The shaded areas in the plots of Figures (5) and (6) correspond to regions that are excluded by the following constraints:

- **Vacuum stability:**

Vacuum stability (at tree level) demands that

$$\begin{aligned} \lambda_{1,2} &> 0, \\ \lambda_3, \lambda_3 + \lambda_4 - |\lambda_5| &> -2\sqrt{\lambda_1 \lambda_2}. \end{aligned} \quad (9)$$

As a result, negative couplings, and $\lambda_L < 0$ among others, are largely excluded. This is the shaded area in the domains $\mu_2 > M_{H_0}$ of Figures (5) and (6).

- **Perturbativity:**

Strong couplings $|\lambda_i| > 4\pi$ are excluded but intermediate couplings, $1 < |\lambda_i| < 4\pi$, might be tolerated. The latter correspond to the regions with horizontal lines. Notice that the mass splitting relative to the μ_2 scale is smaller in the high mass regime (see Eq.(3)). For this reason, going away from the diagonal line in the plots of Figure (6), we run faster into the large coupling regime than in those of Figure (5). The regions excluded by the strong coupling constraint is of course symmetric with respect to the $\mu_2 = M_{H_0}$ axis.

- **Charged Higgs scalar:**

The mass of the charged scalar H^+ is constrained by LEP data to be larger than 79.3 GeV [30]. As we fix the mass differences in our plots, this constraint translates in the excluded region $M_{H_0} \lesssim 30$ GeV in the low mass regime abundance plots.

- **Electroweak Precision Tests (EWPT):**

New physics can affect electroweak precision measurements. The impact of the new H_2 doublet can be described in term of the S , T electroweak precision parameters. As pointed out in [6], with appropriate mass splittings between its components, an H_2 could screen the contribution to the T parameter of a large Higgs masses, $M_h \sim 500$ GeV. The effects on the S parameter is parametrically smaller for the region of parameter space satisfying the previous constraints. In all the case we have studied, we have checked that the contribution to the T parameter resulting from the Higgs mass and the H_2 components are consistent with EWPT. Unlike Barbieri *et al*, we only considered small values of the Higgs mass, $M_h \lesssim 200$ GeV. Given our choice of the Higgs mass M_h and of mass splittings between the H_0 particles and the other components of H_2 , the constraints from EWPT are easily satisfied.

We now turn to the analysis of the model, starting with the low H_0 mass regime.

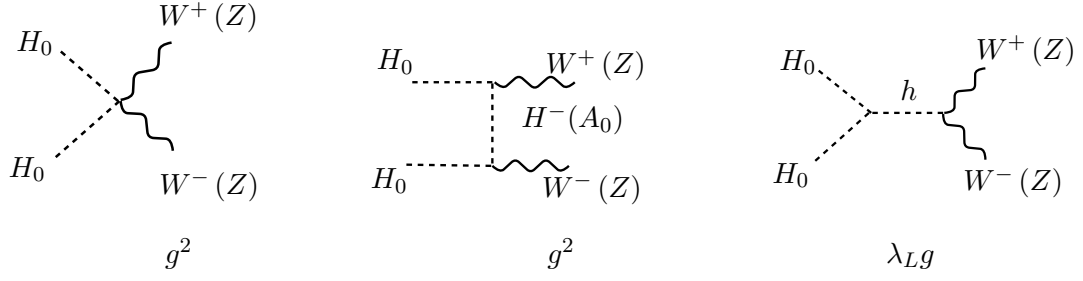


Figure 1: Annihilation channels into gauge bosons final state with corresponding couplings.

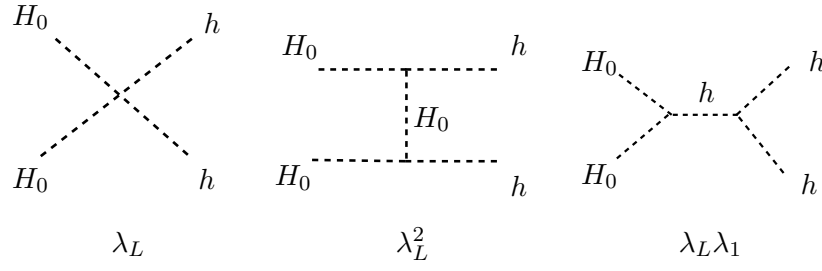


Figure 2: Annihilation channels into Higgs final state.

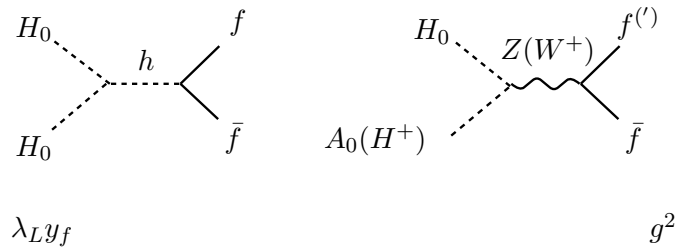


Figure 3: (Co)Annihilation channels into fermion anti-fermion final state.

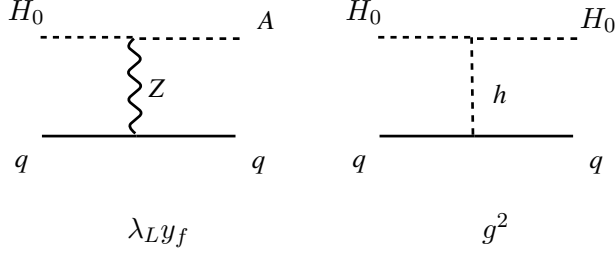


Figure 4: Leading channels contributing to σ_{H_0-p} (direct detection).

3.2 Low mass regime, M_H around 100 GeV

The results of this section are shown in Figure (5). Two processes are relevant below the W , Z or h threshold: H_0 annihilation through the Higgs and H_0 coannihilation with A_0 through Z exchange. Both give fermion-antifermion pairs, the former predominantly into $b\bar{b}$. As the mass of H_0 goes above W , Z or h threshold, H_0 annihilation into WW , ZZ and hh become increasingly efficient, an effect which strongly suppresses the H_0 relic density.

Coannihilation into a Z may occur provided $\Delta M A_0$ is not too important[†], roughly ΔM must be of order of $T_{fo} \sim M_{H_0}/25$. Otherwise H_0 annihilate dominantly into $b\bar{b}$. This regime is quite interesting: the interactions are either completely known (*i.e.* electroweak interactions), or highly sensitive to the Higgs boson mass M_h and the $H_0 h$ effective coupling λ_L !

For the sake of illustration, we study two cases, $M_h = 120$ GeV and $M_h = 200$ GeV to show how the predictions change as a function of the Higgs boson mass. A few general lessons can be extracted from these two specific examples. Note that the mass differences $\Delta M A_0$ and $\Delta M H_c$ are fixed respectively to 10 and 50 GeV while $\Delta M A_0$ is large enough to avoid the constraints from direct detection and small enough to have a some amount of coannihilation into a Z .

We may distinguish five different regions (see Figure (5), top left):

Regions **1** and **2** are excluded respectively by charged Higgs production and vacuum stability constraints. The latter involves the self coupling of the Higgs, λ_1 and thus depends on the Higgs mass (see Eq.(2)): region **2** is broader for smaller Higgs mass M_h . Although region **1** is experimentally ruled out, it is interesting to understand the trends. In this region, the relic abundance of H_0 decreases with increasing M_{H_0} as one goes along $\mu_2 = M_{H_0}$. Comparing the $M_h = 120$ GeV and $M_h = 200$ GeV plots we observe that the gradients depend, again, on the Higgs mass. This is simply due to the $M_{H_0}^2/M_h^4$ dependence of the annihilation cross section through the Higgs, *i.e.* smaller abundance for higher M_{H_0} and/or lower M_h . In region **2**, the abundance is smaller the further one deviates from $\mu_2 = M_{H_0}$, reflecting the dependence of the annihilation cross section on $|\lambda_L|$. For $M_{H_0} \lesssim M_W$ (resp. $M_{H_0} \gtrsim M_h$), $H_0 H_0 \rightarrow b\bar{b}$ (resp. $H_0 H_0 \rightarrow hh$) is the dominant process. Otherwise, for $M_W \lesssim M_{H_0} \lesssim M_h$, $H_0 H_0 \rightarrow WW, ZZ$ dominate.

In region **3**, the couplings are rather large, but nevertheless consistent with vacuum stability. Since $\mu_2 > M_{H_0}$, M_W , the dominant contribution to the cross section is given by $H_0 H_0 \rightarrow W^+ W^-$ process, large enough to bring the relic abundance far below WMAP data.

Region **4** is below the W threshold. It is the only region consistent with the dark matter abundance predicted by WMAP data in the low mass regime. The process that determines the relic abundance of H_0 is again the annihilation through the Higgs. Coannihilation processes become dominant near the resonance at $M_{A_0} + M_{H_0} \approx M_Z$. This is the origin of the dip in the H_0 relic abundance around $M_{H_0} \approx 40$ GeV (corresponding to $M_{A_0} \approx 50$ GeV for our choice of mass splittings). Similarly, annihilation near

[†] $H_0 H^+$ coannihilation is suppressed for our choice of $\Delta M H_c$.

the Higgs resonance generates a second dip around $M_{H_0} \approx M_h/2$. There is an island consistent with WMAP data, which extends up to $M_{H_0} \sim 80$ GeV, at which point WW annihilation becomes important and suppresses the relic abundance.

Region 5, finally, corresponds to $M_{H_0} > M_W$. Annihilation into a gauge boson pair is dominant, at least as long as $M_{H_0} < M_h$. Gauge boson pair production dominates above the Higgs threshold for $\mu_2 < M_{H_0}$ while Higgs pair production is dominant if $\mu_2 > M_{H_0}$. In all instances, the relic abundance is too suppressed to be consistent with WMAP for $M_{H_0} \lesssim 600$ GeV.

As expected, and as revealed by visual inspection, the photon flux plots shares some of the characteristics of the abundance plots. The only new salient feature is the absence of a dip at the Z resonance. This is of course because today, in contrast with the early universe, all A_0 are gone. Existing experiments are not very constraining but future gamma ray detection experiments, such as GLAST, might severely challenge the model. As usual we should bear in mind the astrophysical uncertainties: by changing the galactic dark matter density profile, we can get higher (or smaller) fluxes.

The plot of the cross section for direct detection is pretty transparent. Suffices to notice (see section 2.3) that σ_{H_0-p} at tree level is proportional to λ_L^2 . The dominant contribution to the elastic scattering cross section is thus zero on the $\mu_2 = M_{H_0}$ axis while it increases for larger values of $|\mu_2 - M_{H_0}|$.

The dependence on the Higgs mass (Eq. 8) clearly appears when comparing the σ_{H_0-p} plots for $M_h = 120$ GeV and $M_h = 200$ GeV. For $M_{H_0} > M_W$, the one-loop contribution to the cross section from W exchange is taken into account. However it does not affect much the results as it only amounts for 10^{-13} pb. Unless we suppose that the mass of H_0 and A_0 are nearly degenerate, existing direct detection experiments are not very constraining. Forthcoming experiments however might put a dent on some of the solutions consistent with WMAP.

3.3 The high mass regime, $M_H \gg M_W$

The results of this section are shown in Figure (6), left column. No new annihilation channel opens if M_{H_0} is heavier than the Higgs or gauge bosons. There are then essentially two sort of processes which control both the abundance and the gamma ray flux: the annihilation into two gauge bosons, dominant if $\mu_2 < M_{H_0}$, and the annihilation into two Higgs, which dominates if $\mu_2 > M_{H_0}$. Coannihilation plays little role. It affects a bit the relic abundance along the diagonal but, even so, it is not the key process to get the WMAP abundance.

The abundance of dark matter is suppressed over most of the area of the plot because of large quartic coupling effects on the cross sections. Strong couplings are excluded on a physical basis, but we found this limit nevertheless useful to understand the interplay between the various processes. In the present subsection, we will argue that it is possible to reach agreement with WMAP data, but only to the price of some fine tuning between the different annihilation channels.

Consider first the annihilation into two Higgs bosons (the dashed line in the graphs Figure (7)). Its cross section is vanishing for $\lambda_L = 0$. For $\mu_2 < M_{H_0}$ (corresponding to $\lambda_L > 0$), there is a destructive interference between the diagrams of Figure (2), which is absent if $\mu_2 > M_{H_0}$. The annihilation into gauge bosons depends on the quartic couplings between the scalars (see Figure (1)). Indeed, the annihilation through an intermediate Higgs is controlled by λ_L . Also, the t and u channels exchange diagrams are sensitive to the mass differences between the components of the H_2 doublet, which depend respectively on λ_5 for the annihilation into Z bosons and on $\lambda_4 + \lambda_5$ for the annihilation into W bosons.

If $\lambda_L \simeq 0$, there is no or little annihilation into a Higgs. The relevant diagrams are then the quartic vertex with two gauge bosons and the t and u channels with A_0 (resp. H^+) exchange. If $\lambda_5 = 0$ (resp. $\lambda_4 + \lambda_5 = 0$) the cross section into a Z (resp. W) boson pair is minimal and scales like $\alpha_W^2/M_{H_0}^2$. If, for instance, $\lambda_5 \neq 0$ the annihilation into a Z boson pair receives a contribution which grows like $\alpha_W^2(M_{A_0} - M_{H_0})^2/M_Z^4$. A similar result holds for the annihilation into a W boson pair provided $\lambda_4 + \lambda_5 \neq 0$. Notice that $\alpha_W^2(M_{A_0} - M_{H_0})^2/M_Z^4 \sim \lambda_5^2/M_{H_0}^2$. The effects of weak isospin breaking between the components of H_2 is reminiscent of what happens for the Higgs in the regime of strong λ_1 coupling (the so-called Goldstone boson equivalence theorem [31]).

To have an abundance of dark matter in agreement with WMAP, the mass splittings between the components of H_2 must be kept relatively small. First because large mass splittings correspond to large couplings and second because the different contributions to the annihilation cross section must be suppressed at the same location, around $\lambda_L = 0$ (*ie* $M_{H_0} \simeq \mu \simeq M_{A_0} \simeq M_{H_+}$ in this case). This is illustrated in Figure (7) for two different mass splittings. The first plot is for small mass differences ($\Delta M_{A_0} = 5$ GeV and $\Delta M_{H_c} = 10$ GeV), the second one for (relatively) larger splittings ($\Delta M_{A_0} = 10$ GeV and $\Delta M_{H_c} = 50$ GeV). In the second case, the cross section is too large to obtain an abundance consistent with WMAP, $\langle \sigma v \rangle_{\text{WMAP}} \sim \text{pb}$.

In the limit of small mass splittings and vanishing $\lambda_L = 0$ we have the right amount of dark matter provided $M_{H_0} \gtrsim 600$ GeV. This regime corresponds to the narrow region around the diagonal in Figure (6). The abundance increases for increasing M_{H_0} , but this can be somewhat compensated by playing with the mass splittings, which, as discussed above, tend to increase the cross section. For instance, for $\Delta M_{A_0} = 5$ GeV and $\Delta M_{H_c} = 10$ GeV, we get the right relic abundance for $M_{H_0} \gtrsim 800$ GeV.

There is however a limit to this trend. Indeed, the total annihilation cross section of a scalar particle, like our H_0 , is constrained by unitarity to be smaller than

$$\langle \sigma v \rangle_{v \rightarrow 0}^{\text{unit}} \approx \frac{4\pi}{M_{H_0}^2} \sqrt{\frac{x_f}{\pi}} \quad (10)$$

a result which, in the context of dark matter relics from freeze-out, has been first put forward by Griest and Kamionkowski [32]. In the present model, increasing the mass splitting drives the annihilation cross section toward the strong quartic coupling regime. A similar result holds, for instance, for a weakly interacting massive neutrino candidate of dark matter. In this case, both the neutrino and its charged partner should be kept lighter than, say 1 TeV, since their mass comes from Yukawa couplings to the Higgs field. (See [33] and the discussion in [32]). In our case, the bulk of the mass of the components of the H_2 doublet comes from the mass scale μ_2 , which is *a priori* arbitrary. However, the unitarity limit and WMAP data constraints, translate into the upper bound $M_{H_0} \lesssim 130$ TeV [32].

Unfortunately neither direct, nor indirect detection experiments are sensitive to the large mass region discussed in this section. Forthcoming direct detection experiments might do better, but as the plots show rather clearly, other forms of dark matter would then have to be introduced in order to explain the amount of dark matter that is currently observed. However, if the profile of dark matter in the galaxy is as assumed in the present paper (*ie*. NFW), future gamma detectors (GLAST) will probe most of the parameter space considered in this section, keeping in mind that we had to finely tune the mass splittings to obtain the right abundance.

4 Conclusions

The dark matter candidate of the Inert Doublet Model stands fiercely by the neutralino. The lightest stable scalar is a weakly interacting massive particle with a rich, yet simple, phenomenology and it has a true potential for being constrained by existing and forthcoming experiments looking for dark matter. For the sake of comparison, we show in the right part of Figure (6) a fair sample of models, both for the IDM and the MSSM. In the $(M_{DM}, \Omega_{DM} h^2)$ plane, we clearly see the two regimes (low mass and high mass) of the IDM that may give rise to a relevant relic density (*ie* near WMAP). The MSSM models have a more continuous behavior, with $\mathcal{O}(100 \text{ GeV})$ dark matter masses. For indirect detection, the IDM dark matter candidates have typically higher detection rates than the neutralino in SUSY models, especially at high mass. It is in particular interesting that the IDM can give the right relic abundance in a range of parameters which will be probed by GLAST. Direct detection is also promising but only at low masses, where the models are within reach of future ton-size experiments. The high mass models, however, have too small cross sections in the regions consistent with WMAP.

The phenomenology of the IDM candidate for dark matter is intertwined with that of the Brout-Englert-Higgs particle, h . It could be of some interest to investigate the prospect for detection of the h and H_2 components at the LHC, in the light of the constraints for dark matter discussed in the present paper.

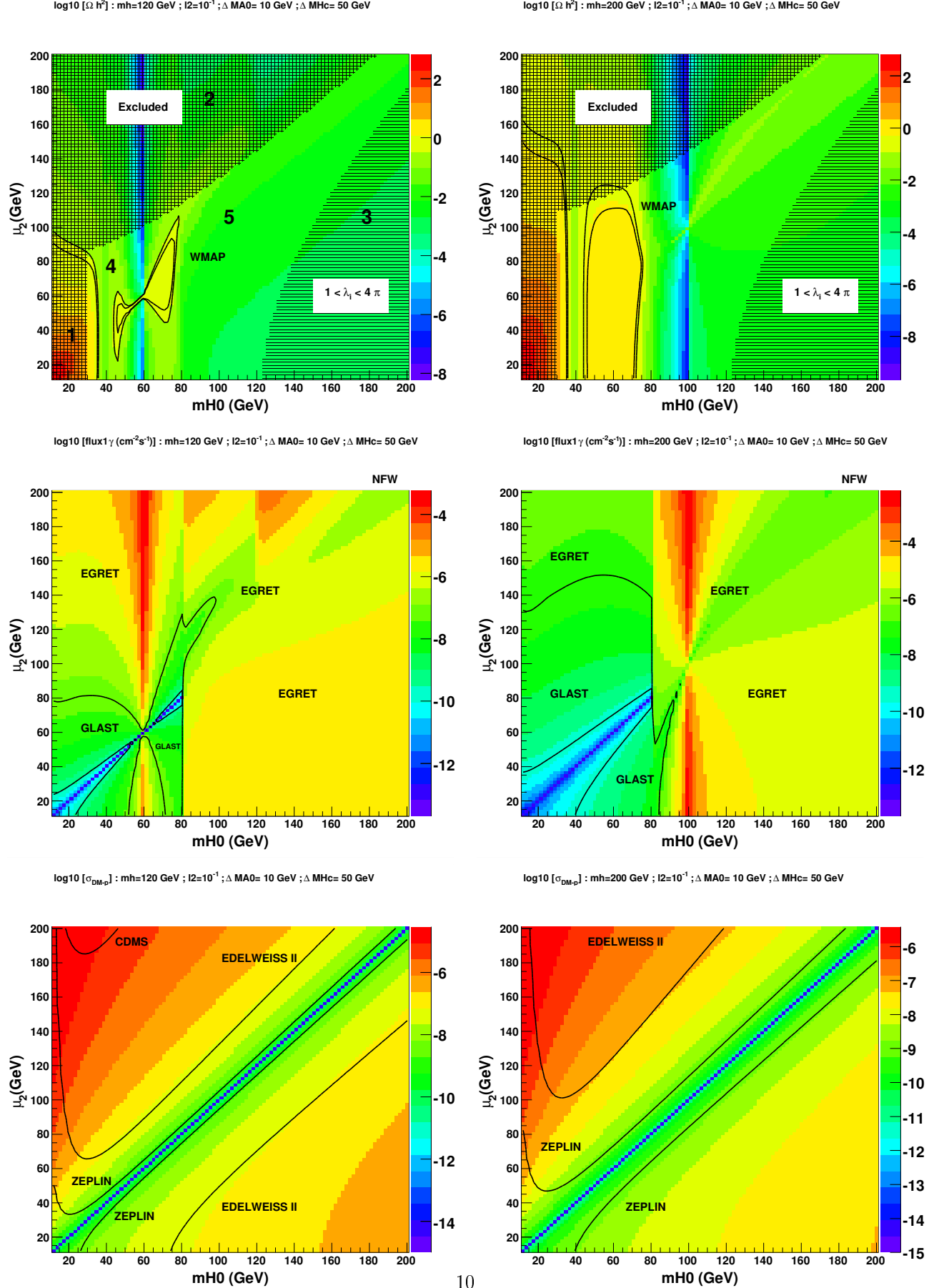


Figure 5: From top to bottom: Relic density, gamma indirect detection and direct detection contours in the (M_{H_0}, μ_2) plane. Left: $m_h = 120$ GeV. Right: $m_h = 200$ GeV.

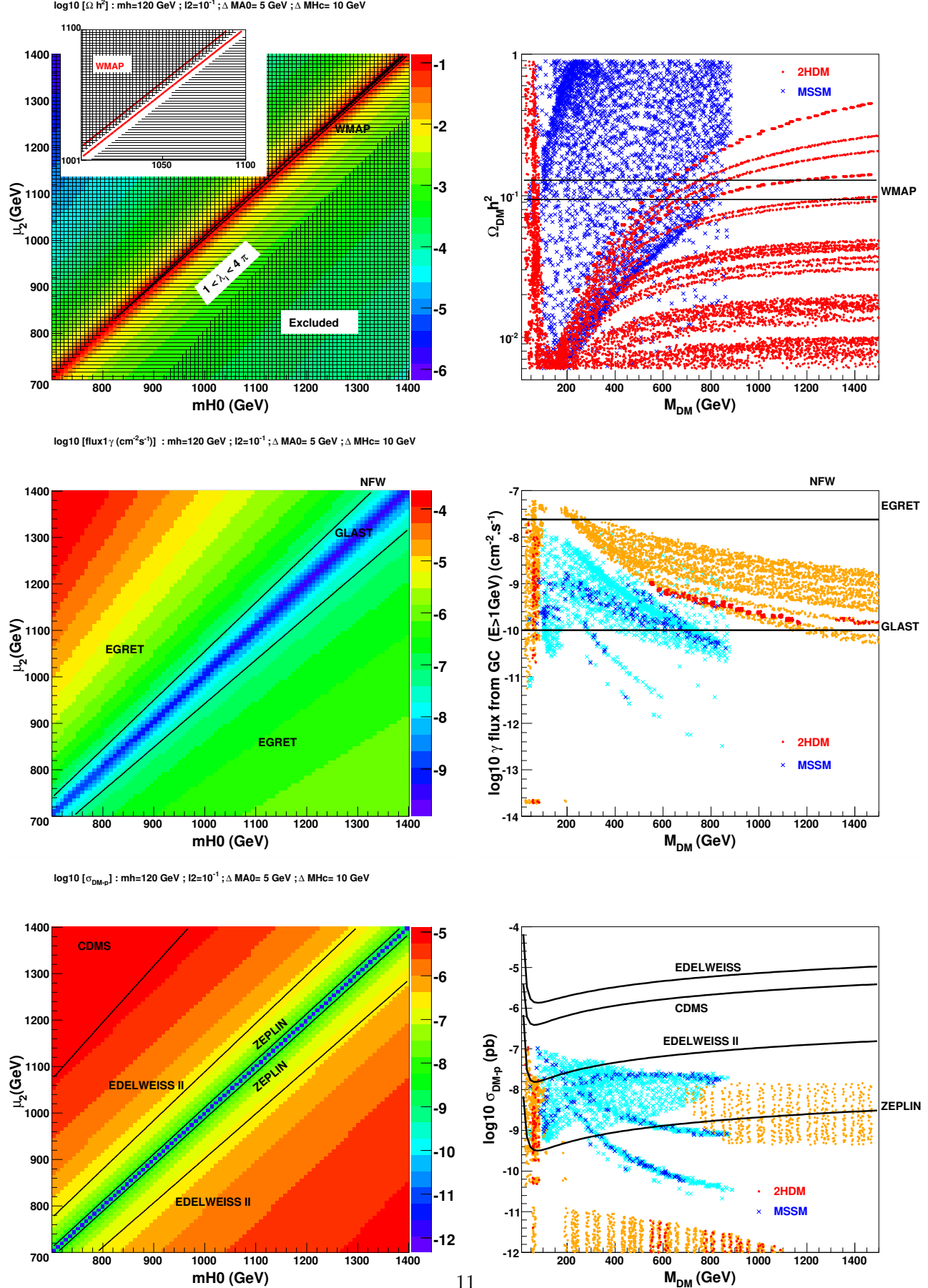


Figure 6: Left: same as Figure (5) for $M_{H_0}, \mu_2 \in [700, 1400]$ GeV. Right: Comparison with the MSSM. From top to bottom: Relic density, gamma indirect detection, direct detection, all as a function of the

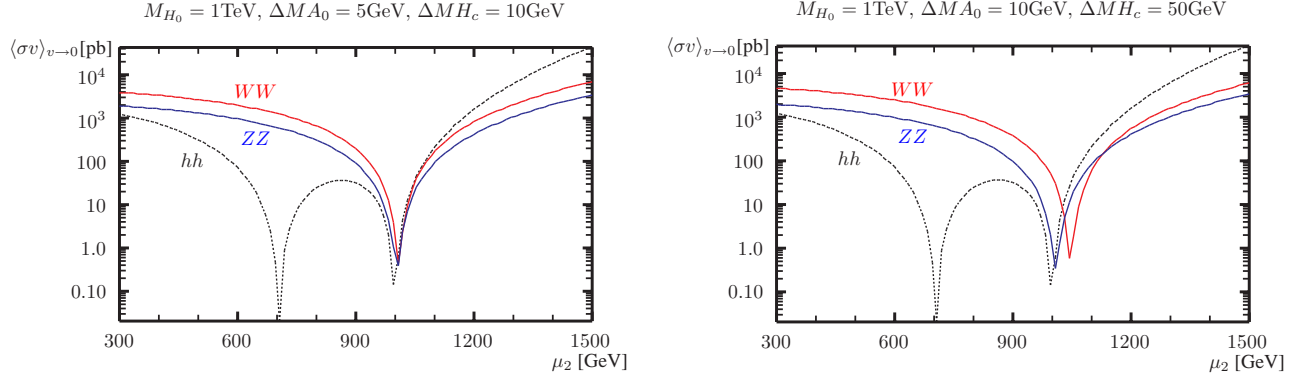


Figure 7: $\langle\sigma v\rangle_{v\rightarrow 0}$ as a function of μ_2 for $M_{H_0} = 1000$ GeV and small mass splittings $\Delta M A_0 = 5$ GeV, $\Delta M H_c = 10$ GeV for the plot on the left and larger mass splittings $\Delta M A_0 = 10$ GeV, $\Delta M H_c = 50$ GeV for the plot on the right. Dashed line corresponds to annihilation into two Higgs, continuous lines to annihilation into two gauge bosons.

Acknowledgments

This work is supported by the FNRS, the I.I.S.N. and the Belgian Federal Science Policy (IAP 5/27).

References

- [1] D. N. Spergel *et al.*, arXiv:astro-ph/0603449.
- [2] U. Seljak, A. Slosar and P. McDonald, JCAP **0610** (2006) 014 [arXiv:astro-ph/0604335].
- [3] G. Bertone, D. Hooper and J. Silk, Phys. Rept. **405** (2005) 279 [arXiv:hep-ph/0404175].
- [4] G. Jungman, M. Kamionkowski and K. Griest, Phys. Rept. **267** (1996) 195 [arXiv:hep-ph/9506380].
- [5] E. Ma, Phys. Rev. D **73** (2006) 077301 [arXiv:hep-ph/0601225].
- [6] R. Barbieri, L. J. Hall and V. S. Rychkov, Phys. Rev. D **74** (2006) 015007 [arXiv:hep-ph/0603188].
- [7] M. Cirelli, N. Fornengo and A. Strumia, arXiv:hep-ph/0512090.
- [8] N. G. Deshpande and E. Ma, Phys. Rev. D **18** (1978) 2574.
- [9] D. Majumdar and A. Ghosal, arXiv:hep-ph/0607067.
- [10] J. A. Casas, J. R. Espinosa and I. Hidalgo, arXiv:hep-ph/0607279.
- [11] X. Calmet and J. F. Oliver, arXiv:hep-ph/0606209.
- [12] J. Kubo, E. Ma and D. Suematsu, arXiv:hep-ph/0604114.
- [13] T. Hambye, K. Kannike, E. Ma and M. Raidal, arXiv:hep-ph/0609228.
- [14] E. Ma, Mod. Phys. Lett. A **21** (2006) 1777 [arXiv:hep-ph/0605180].
- [15] K. Griest and D. Seckel, Phys. Rev. D **43**, 3191 (1991).
- [16] G. Belanger, F. Boudjema, A. Pukhov and A. Semenov, arXiv:hep-ph/0607059.
- [17] J. Edsjo and P. Gondolo, Phys. Rev. D **56**, 1879 (1997) [arXiv:hep-ph/9704361].
- [18] EGRET Collaboration, S. D. Hunger et al., *Astrophys. J.* **481** (1997) 205; H. A. Mayer-Hasselwander et al., *Astron. & Astrophys.* **335** (1998) 161.
- [19] N. Gehrels, P. Michelson, *Astropart. Phys.* **11** (1999) 277;
See also the web page <http://www-glast.stanford.edu>

- [20] J.F. Navarro, C.S. Frenk, S.D.M. White, *Astrophys. J.* **490**, 493 (1997).
- [21] B. Moore *et al.*, *Mon. Not. Roy. Astron. Soc.* **310**, 1147-1152 (1999).
- [22] E. Athanassoula, F. S. Ling and E. Nezri, *Phys. Rev. D* **72**, 083503 (2005) [arXiv:astro-ph/0504631].
- [23] Y. Mambrini, C. Munoz, E. Nezri and F. Prada, *JCAP* **0601**, 010 (2006) [arXiv:hep-ph/0506204].
- [24] M. W. Goodman and E. Witten, *Phys. Rev. D* **31**, 3059 (1985).
- [25] J. R. Ellis, A. Ferstl and K. A. Olive, *Phys. Lett. B* **481**, 304 (2000) [arXiv:hep-ph/0001005].
- [26] CDMS Collaboration, R. Abusaidi et al., *Phys. Rev. Lett.* **84** (2000) 5699; *Phys. Rev. D* **66** (2002) 122003.
- [27] <http://edelweiss.in2p3.fr>
- [28] R. Luscher. "Dark Matter at Boulby Mine," arXiv:astro-ph/0305310.
Talk given to the XXXVIIIth Rencontres de Moriond Electroweak Interactions and Unified Theories, 15th to March 22nd 2003, Les Arcs France.
- [29] M. Sher, *Phys. Rept.* **179**, 273 (1989).
- [30] Particle Data Group, <http://pdg.lbl.gov>, Searches for Higgs Bosons.
- [31] M. E. Peskin and D. V. Schroeder, "An Introduction To Quantum Field Theory," Addison-Wesley (1995).
- [32] K. Griest and M. Kamionkowski, *Phys. Rev. Lett.* **64** (1990) 615.
- [33] K. Enqvist, K. Kainulainen and J. Maalampi, *Nucl. Phys. B* **317** (1989) 647.